NACA RM L56I27

NACA

RESEARCH MEMORANDUM

TRANSONIC FLUTTER INVESTIGATION OF TWO 64° DELTA WINGS WITH SIMULATED STREAMWISE RIB AND ORTHOGONAL SPAR CONSTRUCTION

By George W. Jones, Jr., and Lou S. Young, Jr.

Langley Aeronautical Laboratory
Langley Field, Va.

NATIONAL ADVISORY COMMITTEE
FOR AERONAUTICS
WASHINGTON

January 4, 1957
Declassified April 12, 1961

NATIONAL ADVISORY COMMITTEE FOR AERONAUTICS

RESEARCH MEMORANDUM

TRANSONIC FLUTTER INVESTIGATION OF TWO 64° DELTA WINGS WITH SIMULATED STREAMWISE RIB AND ORTHOGONAL SPAR CONSTRUCTION

By George W. Jones, Jr., and Lou S. Young, Jr.

SUMMARY

An experimental investigation has been made in the Langley transonic blowdown tunnel of the transonic flutter characteristics of two 64° swept-back delta wings. Each wing had simulated streamwise ribs and orthogonal spanwise spars, but one wing had a different stiffness and mass than the other. Flutter was obtained on the more flexible wing at several Mach numbers from 0.79 to 1.28 and on the stiffer wing at Mach numbers from 0.84 to 0.97.

At a given Mach number, the value of the mass ratio at flutter differed for the two wings by a factor up to 2, but the data were correlated by use of a parameter consisting of the flutter-speed coefficient divided by the square root of the mass ratio. As the Mach number was increased, the dynamic pressure required for flutter and the flutter frequency increased by a factor of about 2 at a Mach number of approximately 1.05; this increase is interpreted as a change in flutter mode. Reference flutter speeds were calculated by use of streamwise two-dimensional incompressible aerodynamic coefficients in a coupled modal analysis. These calculated flutter speeds were too high for the low-frequency flutter mode by 11 to 28 percent and too low for the high-frequency flutter mode by 11 to 35 percent.

INTRODUCTION

Although delta-wing plan forms are in present-day and projected use for high-speed aircraft, little is known about the transonic flutter characteristics of this type of wing configuration. An exploratory investigation has accordingly been made in an attempt to define some of the transonic flutter problems of delta wings. The investigation, which was made in the Langley transonic blowdown tunnel, consisted of transonic flutter

tests on a 64° delta-wing plan form (aspect ratio about 2) which simulated in a crude manner one of several general types of delta-wing construction in present-day use.

The model construction simulated spars normal to the fuselage plane of symmetry and streamwise ribs. Flutter points were obtained in the Mach number range from 0.79 to 1.28 with the model cantilever mounted at zero angle of attack without body freedoms. The effect of variations in the mass ratio was determined at subsonic speeds by use of a second, stiffer model which also had simulated streamwise ribs with orthogonal spars.

The results of the investigation are presented herein together with a comparison of the experimental flutter speeds with those calculated by a simplified method. Also included is a comparison of the measured vibration modes with those calculated from measured structural influence coefficients.

SYMBOLS

a	streamwise distance from strip reference axis to strip center-of-gravity location, positive if center of gravity is behind reference axis, ft
b	streamwise strip semichord passing through influence coefficient stations on strip, ft
b_r	reference wing streamwise semichord, mean geometric exposed semichord, ft
f_i	measured coupled natural frequencies (i = 1, 2, 3, or 4), cps
g_h	structural damping coefficient in bending
h_i	contribution of the ith linearized mode to nondimensional vertical displacement of a wing strip reference axis (i = 1, 2, or 3)
$I_{\alpha\delta}$	mass moment of inertia of streamwise wing strip of width δ about the strip reference axis, slug-ft^2
M	Mach number
$m\delta$	mass of a streamwise wing strip of width δ, slugs
m_s	mass of wing sections (s = 1, 2, 3, . . ., 20), slugs, (fig. 4)
q	dynamic pressure, $\frac{1}{2}\rho V^2$, lb/sq ft

$S_\alpha\delta$ static mass moment of streamwise wing strip of width δ about strip reference axis, positive if center of gravity is behind reference axis, slug-ft

t/c ratio of wing thickness to streamwise chord

V free-stream velocity, ft/sec

V_e/V_R flutter-speed ratio, ratio of experimental flutter speed to calculated, or reference, flutter speed

x_{cg} streamwise distance from leading edge to center-of-gravity position, fraction of streamwise chord

y vertical deflection of wing

y_s vertical deflection of wing at a point where an influence coefficient was measured ($s = 1, 2, 3, \ldots, 20$)

α_i contribution of the ith linearized mode to torsional deflection of a wing strip about the strip reference axis ($i = 1, 2,$ or 3)

δ width of wing strip used for reference flutter-speed calculations, ft

η nondimensional distance along exposed wing span, $\dfrac{\text{Spanwise distance measured from wing root}}{\text{Length of exposed span}}$

μ mass-ratio parameter, $\dfrac{\text{Exposed panel mass}}{(\text{Exposed panel span})\left(\pi\rho b_r^2\right)}$

Λ sweepback angle of leading edge, deg

ρ air density, slugs/cu ft

ω angular frequency of flutter, radians/sec

ω_i angular coupled natural frequencies, $2\pi f_i$, radians/sec

ω_α angular coupled predominately torsion frequency, ω_3, radians/sec

Subscripts:

e experimental values

R calculated values

MODELS

Wing Geometry

A sketch of both delta wings showing plan forms, basic dimensions, and construction is given in figure 1. Each wing had a leading-edge sweepback angle of approximately 64° and tips clipped along streamwise lines. The wing sections had a rounded leading edge over the first 4 percent chord, straight parallel top and bottom surfaces to 85 percent chord, and a straight taper on top and bottom from 85 percent chord to a sharp trailing edge. Along the span each wing panel had a nearly constant ratio of thickness to chord except that near the tip the thickness ratio increased somewhat. (See fig. 2.)

Wing Construction

Each of the wings was constructed from a blank of 2024 aluminum alloy which was shaped into two panels, as described in the previous section, with an integral mounting block, as shown in figure 1. One panel of each wing was modified so as to roughly simulate spars normal to the fuselage plane of symmetry and streamwise ribs. The formation of the simulated ribs and spars was accomplished by cutting a pattern of circular holes, some of which were connected by streamwise saw cuts, through the solid 2024 wing panel. On both modified wing panels the holes and cuts were filled with lightweight, low-stiffness foam plastic and wrapped with a sheet of 0.003-inch-thick fiber glass. Figure 1 shows that wing 2 has a pattern of streamwise saw cuts which is different from that of wing 1. The difference in patterns of the saw cuts changed the number and location of the simulated spars and, along with a slightly greater thickness for wing 2, resulted in wing 2 being stiffer than wing 1.

Wing Physical Parameters

Measurements were made on wings 1 and 2 of the first four coupled natural frequencies and node lines, the exposed panel mass, and the structural damping coefficient in bending. Values of the structural damping coefficient were determined from the decrement of free-bending vibrations in still air. The measured frequencies and node lines which

are presented in figure 3 were obtained by use of an electromagnetic shaker mounted close to the root (see fig. 3); sprinkled salt crystals depicted the node lines at the natural frequencies. On the basis of repeatability of the data the measured frequencies have an accuracy which varies from about 1 percent for the lowest frequency to about 2 percent for the fourth frequency. The calculated node lines and frequencies of wing 1 which are shown in figure 3 will be discussed subsequently.

Structural influence coefficients were measured at 15 points on wing 1. The values of the influence coefficients obtained are given in table I(a). The points at which the influence coefficients were measured are shown in figure 4 which will be discussed in more detail later.

Each influence coefficient was obtained in the following manner: The wing was firmly clamped in a horizontal plane to a massive mount. A traveling overhead support held a depth micrometer which was used to measure the deflections of the wing. The micrometer could be read directly to the nearest ten-thousandth of an inch and interpolated to the nearest fifty-thousandth of an inch. In order to ascertain when the pointed end of the micrometer (radius about 0.015 inch) touched the wing surface, a direct current electrical circuit containing a neon test lamp was rigged between the wing surface (which was coated with a conducting silver paint) and the micrometer point. When the point touched the wing, the neon test lamp lit and a reading was taken. A spark jump as the point neared the wing was virtually eliminated by a high resistance in the circuit. A micrometer reading was made of the wing position with no load on the wing, then a weight was hung at the desired station and another reading was taken. The loading-deflection reading procedure was repeated several times for each influence coefficient. The deflections thus obtained were averaged and then adjusted to give deflection per unit load.

For use in frequency calculations the matrix of table I(a) was made symmetrical by the following procedure: Each influence coefficient of table I(a) was weighted (multiplied) by the number of deflections averaged to obtain it. Then the sum of each weighted pair of supposedly reciprocal influence coefficients was divided by the total of the weighting factors to give the final influence coefficient value. Influence coefficients at five additional stations (fig. 4) near the root were interpolated from the adjusted measured values and assumed zero deflection at the root. The final matrix of adjusted and interpolated influence coefficients used for frequency calculations is given in table I(b). In table I(a), 78 percent of the off-diagonal elements were within 3 percent of their corresponding adjusted values in table I(b), and 92 percent were within 6 percent.

After testing, the exposed modified panel of wing 1 was cut into six streamwise strips; and the mass, the mass moment of inertia about the assumed strip reference axis, and the center-of-gravity location of each strip were determined. The methods used to measure these parameters are discussed in reference 1. Each of the wing strips was then cut into sections associated with the influence coefficients and the masses and center-of-gravity locations of the sections were determined.

The division of wing 1 into strips and sections, the points at which influence coefficients were measured and inferred, the assumed strip reference axes, the section center-of-gravity locations, and a list of section masses are given in figure 4. Table II gives physical parameters of the wings as follows: Table II(a) lists some basic physical properties of wings 1 and 2; table II(b) lists the measured mass properties of wing 1; and table II(c) lists some computed deflection properties of wing 1 which will be discussed subsequently.

APPARATUS AND TESTS

The instrumentation, tunnel characteristics, and testing technique are described in detail in reference 1; only a brief description of these items is given in the following paragraphs.

The flutter tests were made in the Langley transonic blowdown tunnel which has a slotted octagonal test section measuring 26 inches between flats. During the operation of the tunnel, a selected Mach number from subsonic Mach numbers up to supersonic Mach numbers of about 1.4, which is set by an orifice plate downstream of the test section, can be held approximately constant (after the orifice is choked) while test-section pressure, and thus density, is varied. The density range is approximately 0.001 to 0.012 slug per cubic foot.

The delta-wing models were cantilever mounted at 0° angle of attack in a cylindrical sting fuselage mount which covers the mounting block shown in figure 1. The sting fuselage mount extends without change of diameter into the subsonic-flow region of the tunnel and thus prevents the formation of bow shock waves which might reflect from the walls onto the model. The fundamental bending frequency of the sting fuselage mount with model attached is approximately 15 cycles per second.

Basically, the instrumentation was as follows: Wire strain gages, located as shown in figure 3, were used to indicate model deflection about two different axes. A recording oscillograph was used to obtain continuous records of the strain-gage signals, tunnel stagnation temperature and pressure, and test-section static pressure. The records of the strain-gage signals were used to determine the start of flutter and the frequency of wing oscillations.

The Mach number range over which flutter was obtained on the wings was from 0.79 to 1.28, but an attempt was made to flutter the wings at Mach numbers up to 1.35 and dynamic pressures up to 4,500 lb/sq ft.

ANALYSIS

Calculation of Frequencies and Mode Shapes

The symmetrical matrix, table I(b), of adjusted and interpolated influence coefficients measured on wing 1 was put into the matrix equation:

$$\left\{y_s\right\} = \omega_i^2[I]\left[m_s\right]\left\{y_s\right\} \tag{1}$$

where I is the matrix of influence coefficients. Equation (1) was solved for the frequencies of the first three coupled natural vibration modes and for the nondimensional vertical deflections of each of the 20 influence-coefficient stations of wing 1 in these three modes. As shown in figure 4, the 20 influence-coefficient stations of wing 1 were generally not located exactly at the center-of-gravity positions of the influence-coefficient sections. As a check, a matrix of influence coefficients at the center-of-gravity positions of the wing sections was inferred graphically from the values of table I(b) and is presented in table III. The matrix equation (eq. (1)) using this matrix was solved for the frequencies and wing section deflections of the first four natural vibration modes. A comparison of the measured frequencies with the two sets of calculated frequencies follows:

Mode	Measured frequency, cps	Results using influence coefficients of table I(b)		Results using influence coefficients of table III	
		Frequency, cps	Deviation, percent	Frequency, cps	Deviation, percent
First	108	107.9	-0.09	108.7	0.65
Second	253	214	-15.3	243	-3.8
Third	342	361	5.5	370	8.1
Fourth	491	-----	------	463	-5.7

From each set of frequency and deflection calculations on wing 1, the node line associated with each calculated frequency was obtained graphically from cross plots of the computed deflection of the wing in that mode. The computed node lines which are shown in figure 3 appear to be in good agreement with the measured node lines.

In figure 5, plots of the calculated vertical deflections of each wing strip of wing 1 in the first three coupled modes computed from the influence coefficients of table I(b) are presented (dashed lines). The deflections shown have been normalized by the extrapolated deflection of the tip of the quarter-chord line. The deflection curves show marked chordwise bending in the second and third mode for some of the strips. In order to simplify the theoretical flutter-speed calculations the chordwise bending of the strips was removed by fitting a root-mean-square straight line to each of the strip deflection curves (solid lines in fig. 5). Since strip 5 has only two influence coefficient stations and strip 6 has one influence coefficient station and an extrapolated slope, the calculated and linearized deflection curves for these strips in figure 5 coincide.

The vertical translation of the strip reference axis and rotation about the reference axis for each wing strip as obtained from the linearized deflection curves are presented in table II(c) for each of the first three coupled modes. The values in table II(c) of the angular deflection about the strip reference axes are normalized by the extrapolated values of the angular deflection of the streamwise tip chord about the tip of the quarter-chord line.

Calculation of Reference Flutter Speeds

Theoretical or reference flutter speeds were calculated for wing 1. These reference flutter speeds were computed by the use of streamwise two-dimensional incompressible aerodynamic coefficients in a coupled modal analysis. The frequencies used in the analysis were the first three measured coupled natural frequencies and the mode shapes used were those of table II(c) which were obtained as discussed in the previous section.

The influence coefficient stations on each strip lie along a streamwise strip chord as shown in figure 4. Each strip reference axis is the line normal to this strip chord at its quarter-chord point. In the reference flutter-speed analysis, since the strip reference axes were effectively the same as if the wing quarter-chord line had been chosen for the reference axis, there was a simplification in the aerodynamic terms.

The equations of motion and the procedure for computing the coefficients of the flutter stability determinant are given in the appendix.

RESULTS

General Comments

For each of the flutter points only the modified wing panel fluttered. The other panel of solid 2024 aluminum was tested simultaneously, but it was too stiff to flutter in the density range of the tunnel.

The operating characteristics of the tunnel were such that frequently during a single test run (a test run is defined as one operation of the tunnel from valve opening to valve closing) the tunnel operating curve of dynamic pressure as a function of Mach number intersected the wing flutter-boundary curve of dynamic pressure required for flutter against Mach number more than once. In such instances, each point of intersection is presented in the data.

Slightly more than half of the start-of-flutter points were readily determined from the oscillograph records. Each of these starts of flutter was characterized by a change from random wing motion to continuous sinusoidal oscillations accompanied by an increase in oscillation amplitude. For these flutter points, when both sets of strain gages were operating, the frequencies of both strain gages were the same at the start of flutter. For the remainder of the flutter points a period of intermittent sinusoidal type of oscillation preceded continuous flutter and obscured the exact start of flutter. Such periods are designated low-damping regions as in reference 1 inasmuch as the sum of the aerodynamic and structural damping is near zero. Where low damping occurred, two data points were selected: one point near the start of the low-damping region and the other near the start of continuous flutter following the low-damping region. Both data points are presented in the tables and figures.

Presentation of Data

The results of the investigation are listed in table IV. The first four columns of the table contain a description of the chronological behavior of the wing during each test run. The first column gives the wing identification number, the second column the number of the run, and the third column the chronological number of each data point during each run. The fourth column contains code letters (defined in table IV) which describe the behavior of the test wing panel at the time of each data point.

Some of the experimental results tabulated in table IV are plotted as functions of Mach number in figures 6, 7, and 8 for both wings 1 and 2. Figure 6 is a plot of dynamic pressure at flutter; figure 7 is a plot of the parameter $\frac{V_e}{b_r\omega_\alpha\sqrt{\mu_e}}$; and figure 8 is a plot of the flutter

frequency normalized by the third natural frequency, which is designated as the predominantly torsion frequency. It should be noted that for the point at Mach number 1.28 in figure 7 the corresponding ratio of frequencies has not been plotted in figure 8 because the flutter frequency was not obtained. A typical history of Mach number and dynamic pressure during a tunnel run is shown for wing 1 in figure 9. Experimental results normalized by analytical results are shown for wing 1 in figures 10 and 11. Figure 10 shows the variation of flutter-speed ratio with Mach number and figure 11 depicts the corresponding variation of the ratio of experimental to calculated flutter frequency with Mach number. In figures 6, 7, and 10 the low-damping regions are indicated by dashed lines which extend from the start-of-low-damping point (marked only by the lower end of the dashed line) to the continuous-flutter point (marked by a symbol at the upper end of the dashed line).

DISCUSSION

As shown in figure 6, flutter was obtained on wing 1 at Mach numbers from 0.79 to 1.28 and values of dynamic pressure from 878 to 4,296 lb/sq ft. Wing 2 was stiffer and slightly heavier than wing 1, so that the dynamic pressure required to flutter wing 2 was nearer the upper limit of the tunnel dynamic-pressure range. Consequently, only four flutter points at Mach numbers from 0.84 to 0.97 were obtained on wing 2 although it was attempted without success to flutter wing 2 at Mach numbers up to 1.2 with dynamic pressure up to about 4,500 lb/sq ft. The dynamic pressure required to flutter wing 2 at a given Mach number was about double that required for wing 1. (See fig. 6.) Table IV shows that at a given Mach number the density and hence the flutter mass ratio μ_e differed for the two wings by a factor up to 2. (Compare, for instance, the values of wing 1, run 13, point 2 with those of wing 2, run 2, point 2 in table IV.) It can also be seen from figure 6 that for wing 1 at low supersonic Mach numbers there is a very sharp rise in dynamic pressure required for flutter. These data can be discussed with more facility by making use of figure 7. In figure 7, for the two wings investigated, the data obtained are shown to be correlated by the parameter $\frac{V_e}{b_r\omega_\alpha\sqrt{\mu_e}}$, which was also employed in reference 1. This fact indicates that, at a given Mach number, the flutter-speed coefficient $\frac{V_e}{b_r\omega_\alpha}$ for the two wings varies nearly linearly with the square root of the mass ratio for these tests. Figure 7 shows for wing 1 at a Mach number of about 1.05 a sharp rise in $\frac{V_e}{b_r\omega_\alpha\sqrt{\mu_e}}$ which corresponds to the similar

rise in q_e in figure 6. This sharp increase is interpreted as a change in flutter mode. Additional evidence that this shift represents a change in flutter mode is presented in figure 8, which shows a distinct jump in the ratio of flutter frequency to torsion frequency at the same low supersonic Mach number as the shifts in figures 6 and 7. Similar shifts in flutter mode on a delta-wing model are reported in reference 2.

The possibility exists that a second shift in flutter mode on wing 1 may have occurred at a Mach number of 1.24 as evidenced by a large jump in dynamic pressure at flutter (see fig. 6) and frequency of flutter (see fig. 8). The frequency ratio for the point at Mach number 1.28 was not shown since the frequency was not obtained from the record; however, the dynamic pressure at flutter for this point is given (fig. 6). The data available are insufficient to draw a conclusion and the faired flutter boundaries of figures 7 and 10 are drawn as though a second shift in flutter mode did not occur.

The values of the flutter frequencies of wing 1 in the low-frequency flutter mode (175 cps to 204 cps) are between the measured first and second natural coupled frequencies, whereas the frequencies of the high-frequency flutter mode (375 cps to 417 cps) are, with one exception, between the measured third and fourth coupled natural frequencies. The one exception - wing 1, run 10, point 4 - shows a flutter frequency of 500 cps.

Special note should be taken of the regime below the flutter boundary for the high-frequency flutter mode. During the tests, because of the tunnel operating characteristics, a start and stop of flutter in the low-frequency mode was always obtained before flutter in the high-frequency mode was encountered. This sequence of wing behavior is illustrated in figure 9 which is a history of tunnel dynamic pressure and Mach number during tunnel run 11 on wing 1. The circled points in figure 9 are taken from the data given for run 11 in table IV. On every run, as dynamic pressure increased in the regime between the stop of flutter in the low-frequency mode and the start of flutter in the high-frequency mode, some random and intermittent oscillations were noted which were followed by a significant intermittent response of the wing to tunnel turbulence (fig. 9). These intermittent oscillations of the wing were of approximately the same frequency as the low-frequency flutter mode. As dynamic pressure increased, intermittent oscillations of the wing at a frequency near that of the high-frequency flutter mode superimposed on the low-frequency oscillations and gradually replaced them (fig. 9). After the high-frequency intermittent oscillations, flutter in the high-frequency mode began and continued up to the highest value of tunnel dynamic pressure reached during the run.

The reference flutter speeds calculated for wing 1 as described in the "Analysis" section had several limitations: The use of two-dimensional

aerodynamic coefficients was unrealistic on such a low-aspect-ratio, highly swept delta wing. The aerodynamic coefficients were also incompressible ones which precluded the possibility of predicting the change in flutter mode which was probably caused by changes in aerodynamic loading with Mach number. In addition, the effects of chordwise bending on the aerodynamic forces, as well as on the inertia and elastic forces, were neglected. In this connection, it might be pointed out that the neglect of chordwise bending distorted the true mode shapes and destroyed the orthogonality relationship so that the off-diagonal terms of the mass matrix which were considered to be zero were actually not zero. Only the first three coupled modes were used in the analysis. Since the frequency of wing flutter in the high-frequency mode was, with one exception, between the frequencies of the third and fourth coupled modes it might be expected that, in addition to the use of correct aerodynamic coefficients, the inclusion of chordwise bending and the fourth and perhaps higher coupled modes in the analysis would be required to predict the flutter characteristics. The inclusion of chordwise bending might also have improved the correlation at low Mach numbers.

In figure 10 the flutter-speed ratios for wing 1, which were obtained by dividing the experimental flutter speeds by the reference flutter speeds, have an average of about 0.72 at Mach number 0.80. The flutter-speed ratios increase with Mach number to a value of approximately 0.90 at Mach number 1.05 where an abrupt shift in V_e/V_R to a value of about 1.13 occurs. After the shift, which is attributed to the change in flutter mode, the flutter-speed ratios increase steadily with Mach number to a value of about 1.35 at Mach number 1.28. As shown by the flutter-speed ratios of figure 10, the reference flutter speeds were too high (unconservative) for the low-frequency flutter mode by 11 to 28 percent and too low for the high-frequency flutter mode by 11 to 35 percent.

Figure 11 shows that agreement between experimental and calculated flutter frequencies in the low-frequency flutter mode (values of ω_e/ω_R around 0.95) is somewhat better than the agreement between experimental and calculated flutter speeds. However, in the high-frequency flutter mode the calculated flutter frequencies were much too low as shown by values of ω_e/ω_R of about 1.9.

CONCLUSIONS

From a transonic flutter investigation of two 64° sweptback delta wings having streamwise ribs and orthogonal, spanwise spars but different stiffnesses and masses, the following conclusions were obtained:

1. At a given Mach number the values of the mass ratio for the two wings differed by a factor up to 2, but the data were correlated by use of the parameter consisting of the flutter-speed coefficient divided by the square root of the mass ratio.

2. On the more flexible wing both the dynamic pressure required for flutter and the flutter frequency suddenly increased by a factor of about 2 at a Mach number of approximately 1.05: This increase is interpreted as a change in flutter mode.

3. Reference flutter speed calculations made for the more flexible wing using streamwise two-dimensional incompressible aerodynamic coefficients in a coupled modal analysis were too high for the low-frequency flutter mode by 11 to 28 percent and too low for the high-frequency mode by 11 to 35 percent.

Langley Aeronautical Laboratory,
National Advisory Committee for Aeronautics,
Langley Field, Va., September 13, 1956.

APPENDIX

EQUATIONS OF MOTION FOR REFERENCE FLUTTER-SPEED CALCULATIONS

The equations of motion used for the reference flutter-speed calculations are derived in reference 3 and are as follows:

$$\left\{A_1\left[1 - \left(\frac{\omega_1}{\omega}\right)^2\left(1 + ig_1\right)\right] + C_{11}\right\}\xi_1 + C_{12}\xi_2 + C_{13}\xi_3 = 0$$

$$C_{21}\xi_1 + \left\{A_2\left[1 - \left(\frac{\omega_2}{\omega}\right)^2\left(1 + ig_2\right)\right] + C_{22}\right\}\xi_2 + C_{23}\xi_3 = 0$$

$$C_{31}\xi_1 + C_{32}\xi_2 + \left\{A_3\left[1 - \left(\frac{\omega_3}{\omega}\right)^2\left(1 + ig_3\right)\right] + C_{33}\right\}\xi_3 = 0$$

where $\xi_i(t) = \xi_{i,o}e^{i\omega t}$ is the generalized coordinate which is a function of time, the amplitude of which expresses how much of each normal mode is included in the general vibratory motion.

The necessary and sufficient condition that solutions for the simultaneous equations of motion exist $\left(\text{other than } \xi_1 = \xi_2 = \xi_3 = 0\right)$ is that the determinant of the coefficients equals zero.

The coefficients in the equations of motion may be broken down as follows:

$$A_1 = \varphi_1 + \varphi_2 + \varphi_3$$

$$A_2 = \varphi_4 + \varphi_5 + \varphi_6$$

$$A_3 = \varphi_7 + \varphi_8 + \varphi_9$$

where the values of φ for wing 1 are as follows:

$$\varphi_1 = \sum mh_1^2\delta = 0.00011499 \qquad \varphi_5 = \sum I_\alpha\alpha_2^2\delta = 0.00000024200$$

$$\varphi_2 = \sum I_\alpha\alpha_1^2\delta = 0.0000018522 \qquad \varphi_6 = 2\sum S_\alpha h_2\alpha_2\delta = -0.0000027734$$

$$\varphi_3 = 2\sum S_\alpha h_1\alpha_1\delta = 0.000012114 \qquad \varphi_7 = \sum mh_3^2\delta = 0.000059833$$

$$\varphi_4 = \sum mh_2^2\delta = 0.00010864 \qquad \varphi_8 = \sum I_\alpha\alpha_3^2\delta = 0.000015351$$

$$\varphi_9 = 2\sum S_\alpha h_3\alpha_3\delta = -0.000026389$$

and the summations are over wing strips 1 through 6. The C_{ij} terms are:

$$C_{11} = \pi\rho\left[\Phi_1 - \frac{F_r}{G_r^2}\Phi_2 + \frac{G_r}{k_r}\Phi_3 - i\left(\frac{1}{k_r}\Phi_4 + \frac{F_r}{k_r}\Phi_3 + \frac{G_r}{k_r^2}\Phi_2\right)\right]$$

$$C_{12} = \pi\rho\left[\Phi_5 - \frac{F_r}{k_r^2}\Phi_6 + \frac{G_r}{k_r}\Phi_7 - i\left(\frac{1}{k_r}\Phi_8 + \frac{F_r}{k_r}\Phi_7 + \frac{G_r}{k_r^2}\Phi_6\right)\right]$$

$$C_{13} = \pi\rho\left[\Phi_9 - \frac{F_r}{k_r^2}\Phi_{10} + \frac{G_r}{k_r}\Phi_{11} - i\left(\frac{1}{k_r}\Phi_{12} + \frac{F_r}{k_r}\Phi_{11} + \frac{G_r}{k_r^2}\Phi_{10}\right)\right]$$

$$C_{21} = \pi\rho\left[\Phi_5 - \frac{F_r}{k_r^2}\Phi_{13} + \frac{G_r}{k_r}\Phi_{14} - i\left(\frac{1}{k_r}\Phi_{15} + \frac{F_r}{k_r}\Phi_{14} + \frac{G_r}{k_r^2}\Phi_{13}\right)\right]$$

$$C_{22} = \pi\rho\left[\Phi_{16} - \frac{F_r}{k_r^2}\Phi_{17} + \frac{G_r}{k_r}\Phi_{18} - i\left(\frac{1}{k_r}\Phi_{19} + \frac{F_r}{k_r}\Phi_{18} + \frac{G_r}{k_r^2}\Phi_{17}\right)\right]$$

$$C_{23} = \pi\rho\left[\Phi_{20} - \frac{F_r}{k_r^2}\Phi_{21} + \frac{G_r}{k_r}\Phi_{22} - i\left(\frac{1}{k_r}\Phi_{23} + \frac{F_r}{k_r}\Phi_{22} + \frac{G_r}{k_r^2}\Phi_{21}\right)\right]$$

$$C_{31} = \pi\rho\left[\Phi_9 - \frac{F_r}{k_r^2}\Phi_{24} + \frac{G_r}{k_r}\Phi_{25} - i\left(\frac{1}{k_r}\Phi_{26} + \frac{F_r}{k_r}\Phi_{25} + \frac{G_r}{k_r^2}\Phi_{24}\right)\right]$$

$$C_{32} = \pi\rho\left[\Phi_{20} - \frac{F_r}{k_r^2}\Phi_{27} + \frac{G_r}{k_r}\Phi_{28} - i\left(\frac{1}{k_r}\Phi_{29} + \frac{F_r}{k_r}\Phi_{28} + \frac{G_r}{k_r^2}\Phi_{27}\right)\right]$$

$$C_{33} = \pi\rho\left[\Phi_{30} - \frac{F_r}{k_r^2}\Phi_{31} + \frac{G_r}{k_r}\Phi_{32} - i\left(\frac{1}{k_r}\Phi_{33} + \frac{F_r}{k_r}\Phi_{32} + \frac{G_r}{k_r^2}\Phi_{31}\right)\right]$$

where F_r and G_r are the Theodorsen functions corresponding to $\frac{1}{k_r}$ and $k_r = \frac{b_r\omega}{V}$ and the values of Φ_i for wing 1 are as follows:

$$\Phi_1 = \varphi_{10} + \varphi_{12} + \frac{3}{8}\varphi_{15} = 0.00049930$$

$$\Phi_2 = 2b_r^2\varphi_{14} = 0.00056098$$

$$\Phi_3 = 2b_r\left(\varphi_{11} + \varphi_{13}\right) = 0.0021970$$

$$\Phi_4 = b_r\left(\varphi_{13} + \varphi_{16}\right) = 0.00015015$$

$$\Phi_5 = \varphi_{17} + \frac{1}{2}\varphi_{19} + \frac{1}{2}\varphi_{22} + \frac{3}{8}\varphi_{23} = -0.00033548$$

$$\Phi_6 = 2b_r^2\varphi_{21} = 0.00032259$$

$$\Phi_7 = 2b_r\left(\varphi_{18} + \varphi_{20}\right) = -0.00062021$$

$$\Phi_8 = b_r\left(\varphi_{20} + \varphi_{24}\right) = 0.000066768$$

$$\Phi_9 = \varphi_{25} + \frac{1}{2}\varphi_{27} + \frac{1}{2}\varphi_{30} + \frac{3}{8}\varphi_{31} = 0.00018040$$

$$\Phi_{10} = 2b_r^2\varphi_{29} = -0.00055175$$

$$\Phi_{11} = 2b_r\left(\varphi_{26} + \varphi_{28}\right) = 0.00062875$$

$$\Phi_{12} = b_r\left(\varphi_{28} + \varphi_{32}\right) = -0.00025036$$

$$\Phi_{13} = 2b_r^2\varphi_{34} = -0.00025457$$

$$\Phi_{14} = 2b_r\left(\varphi_{18} + \varphi_{33}\right) = -0.00094354$$

$$\Phi_{15} = b_r\left(\varphi_{33} + \varphi_{24}\right) = -0.000094898$$

$$\Phi_{16} = \varphi_{35} + \varphi_{37} + \frac{3}{8}\varphi_{40} = 0.00044528$$

$\Phi_{17} = 2b_r^2\varphi_{39} = -0.000027012$

$\Phi_{18} = 2b_r\left(\varphi_{36} + \varphi_{38}\right) = 0.0014210$

$\Phi_{19} = b_r\left(\varphi_{38} + \varphi_{41}\right) = -0.000022526$

$\Phi_{20} = \varphi_{42} + \frac{1}{2}\varphi_{44} + \frac{1}{2}\varphi_{47} + \frac{3}{8}\varphi_{48}$

$= -0.00012882$

$\Phi_{21} = 2b_r^2\varphi_{46} = 0.00078900$

$\Phi_{22} = 2b_r\left(\varphi_{43} + \varphi_{45}\right) = 0.00017566$

$\Phi_{23} = b_r\left(\varphi_{45} + \varphi_{49}\right) = 0.00026864$

$\Phi_{24} = 2b_r^2\varphi_{51} = 0.00029982$

$\Phi_{25} = 2b_r\left(\varphi_{26} + \varphi_{50}\right) = 0.0011821$

$\Phi_{26} = b_r\left(\varphi_{50} + \varphi_{32}\right) = 0.000026320$

$\Phi_{27} = 2b_r^2\varphi_{53} = 0.00017780$

$\Phi_{28} = 2b_r\left(\varphi_{43} + \varphi_{52}\right) = -0.00032604$

$\Phi_{29} = b_r\left(\varphi_{52} + \varphi_{49}\right) = 0.000017796$

$\Phi_{30} = \varphi_{54} + \varphi_{56} + \frac{3}{8}\varphi_{59} = 0.00012599$

$\Phi_{31} = 2b_r^2\varphi_{58} = -0.00036476$

$\Phi_{32} = 2b_r\left(\varphi_{55} + \varphi_{57}\right) = 0.00044084$

$\Phi_{33} = b_r\left(\varphi_{57} + \varphi_{60}\right) = -0.000020573$

The following values of φ for wing 1 can be evaluated from table II (the summations are over strips 1 through 6):

$\varphi_{10} = \sum b^2h_1^2\delta = 0.00042157$

$\varphi_{11} = \sum bh_1^2\delta = 0.0039323$

$\varphi_{12} = \sum b^3h_1\alpha_1\delta = 0.000071649$

$\varphi_{13} = \sum b^2h_1\alpha_1\delta = 0.00051504$

$\varphi_{14} = \sum bh_1\alpha_1\delta = 0.0045975$

$\varphi_{15} = \sum b^4\alpha_1^2\delta = 0.000016207$

$\varphi_{16} = \sum b^3\alpha_1^2\delta = 0.000092856$

$\varphi_{17} = \sum b^2h_1h_2\delta = -0.00031040$

$\varphi_{18} = \sum bh_1h_2\delta = -0.0014930$

$\varphi_{19} = \sum b^3h_1\alpha_2\delta = 0.000026839$

$\varphi_{20} = \sum b^2h_1\alpha_2\delta = 0.00023751$

$\varphi_{21} = \sum bh_1\alpha_2\delta = 0.0026438$

$\varphi_{22} = \sum b^3h_2\alpha_1\delta = -0.000080477$

$\varphi_{23} = \sum b^4\alpha_1\alpha_2\delta = 0.0000046340$

$\varphi_{24} = \sum b^3\alpha_1\alpha_2\delta = 0.000032808$

$\varphi_{25} = \sum b^2h_1h_3\delta = 0.00024453$

$\varphi_{26} = \sum bh_1h_3\delta = 0.0020758$

$\varphi_{27} = \sum b^3h_1\alpha_3\delta = -0.00015097$

$\varphi_{28} = \sum b^2h_1\alpha_3\delta = -0.00080303$

$\varphi_{29} = \sum bh_1\alpha_3\delta = -0.0045219$

$\varphi_{30} = \sum b^3h_3\alpha_1\delta = 0.000056820$

$\varphi_{31} = \sum b^4\alpha_1\alpha_3\delta = -0.000045483$

$\varphi_{32} = \sum b^3\alpha_1\alpha_3\delta = -0.00021057$

$\varphi_{33} = \sum b^2h_2\alpha_1\delta = -0.00041701$

$\varphi_{34} = \sum bh_2\alpha_1\delta = -0.0020863$

$\varphi_{35} = \sum b^2h_2{}^2\delta = 0.00046584$

$\varphi_{36} = \sum bh_2{}^2\delta = 0.0029824$

$\varphi_{37} = \sum b^3h_2\alpha_2\delta = -0.000021208$

$\varphi_{38} = \sum b^2h_2\alpha_2\delta = -0.00010593$

$\varphi_{39} = \sum bh_2\alpha_2\delta = -0.00022138$

$\varphi_{40} = \sum b^4\alpha_2{}^2\delta = 0.0000017402$

$\varphi_{41} = \sum b^3\alpha_2{}^2\delta = 0.000014730$

$\varphi_{42} = \sum b^2h_2h_3\delta = -0.00025049$

$\varphi_{43} = \sum bh_2h_3\delta = -0.00078501$

$\varphi_{44} = \sum b^3h_2\alpha_3\delta = 0.00023529$

$\varphi_{45} = \sum b^2h_2\alpha_3\delta = 0.0011406$

$\varphi_{46} = \sum bh_2\alpha_3\delta = 0.0064663$

$\varphi_{47} = \sum b^3h_3\alpha_2\delta = 0.000015340$

$$\varphi_{48} = \sum b^4\alpha_2\alpha_3\delta = -0.0000097254$$

$$\varphi_{49} = \sum b^3\alpha_2\alpha_3\delta = -0.000052972$$

$$\varphi_{50} = \sum b^2h_3\alpha_1\delta = 0.00031713$$

$$\varphi_{51} = \sum bh_3\alpha_1\delta = 0.0024572$$

$$\varphi_{52} = \sum b^2h_3\alpha_2\delta = 0.00012502$$

$$\varphi_{53} = \sum bh_3\alpha_2\delta = 0.0014572$$

$$\varphi_{54} = \sum b^2h_3{}^2\delta = 0.00024409$$

$$\varphi_{55} = \sum bh_3{}^2\delta = 0.0016278$$

$$\varphi_{56} = \sum b^3h_3\alpha_3\delta = -0.00017737$$

$$\varphi_{57} = \sum b^2h_3\alpha_3\delta = -0.00073542$$

$$\varphi_{58} = \sum bh_3\alpha_3\delta = -0.0029894$$

$$\varphi_{59} = \sum b^4\alpha_3{}^2\delta = 0.00015805$$

$$\varphi_{60} = \sum b^3\alpha_3{}^2\delta = 0.00065213$$

REFERENCES

1. Unangst, John R., and Jones, George W., Jr.: Some Effects of Sweep and Aspect Ratio on the Transonic Flutter Characteristics of a Series of Thin Cantilever Wings Having a Taper Ratio of 0.6. NACA RM L55I13a, 1955.

2. Herr, Robert W.: A Preliminary Wind-Tunnel Investigation of Flutter Characteristics of Delta Wings. NACA RM L52B14a, 1952.

3. Scanlan, Robert H., and Rosenbaum, Robert: Introduction to the Study of Aircraft Vibration and Flutter. The Macmillan Co., 1951.

TABLE I.- INFLUENCE COEFFICIENTS ON WING 1

Deflection points	Load Points																			
	1	2	3	4	5	6	7	8	9	10	11	12	13	14	15	16	17	18	19	20
(a) Measured influence coefficients, $\frac{ft}{lb} \times 10^5$																				
1																				
2																				
3																				
4																				
5																				
6						3.50	2.03	0.917	0.611	0.444	4.41	2.13	1.47	0.832	3.40	1.90	1.62	2.84	3.00	2.95
7						1.88	3.33	1.75	1.11	.693	7.43	4.08	2.92	1.33	6.52	4.34	3.12	7.12	5.84	8.50
8						.582	2.17	4.42	2.36	1.78	5.04	8.42	6.64	5.12	12.2	10.8	8.07	14.5	13.2	14.6
9						.662	1.02	2.33	4.75	5.64	2.72	6.62	12.8	14.6	10.3	15.3	21.3	19.1	31.3	29.8
10						.428	.763	1.63	5.38	40.3	1.50	3.48	16.4	50.0	7.41	20.9	51.7	25.8	55.8	56.8
11						4.28	7.43	4.88	2.61	1.58	20.2	15.2	8.67	5.20	27.0	17.2	11.7	27.3	20.2	26.6
12						2.40	4.63	8.05	6.41	4.00	15.0	21.6	17.8	15.1	39.8	36.2	29.0	52.2	44.7	54.9
13						1.23	2.69	6.22	12.8	15.7	8.42	19.9	36.8	42.5	36.2	60.2	72.2	79.5	99.2	116
14						.785	1.44	4.38	14.9	48.6	5.58	14.8	43.8	134	27.3	70.3	175	93.3	200	202
15						3.31	6.49	11.5	10.2	7.05	28.0	42.4	36.9	27.7	82.9	75.0	58.8	109	97.5	115
16						1.83	4.44	10.1	16.7	20.2	16.9	35.2	60.2	71.1	70.3	120	136	180	209	260
17						1.32	3.28	7.93	20.8	50.6	11.3	28.6	70.8	174	57.8	135	328	202	455	513
18						3.03	6.72	14.0	20.2	25.8	27.1	54.0	82.8	93.3	110	188	202	337	348	471
19						2.53	5.38	13.0	28.3	56.8	21.2	47.5	102	201	99.2	212	452	354	833	1,170
20						2.80	7.08	14.2	29.5	52.7	24.2	54.8	112	202	118	254	505	468	1,200	1,960
(b) Adjusted and interpolated influence coefficients, $\frac{ft}{lb} \times 10^5$																				
1	0.125	0.100	0.0830	0.00667	0.000833	0.220	0.153	0.0650	0.0580	0.0325	0.221	0.150	0.0875	0.0658	0.199	0.133	0.090	0.175	0.173	0.174
2		.108	.0370	.0117	.0108	.167	.250	.108	.142	.0750	.417	.250	.167	.158	.367	.333	.150	.375	.358	.383
3			.125	.0292	.00833	.0417	.0833	.225	.242	.108	.225	.417	.317	.250	.383	.358	.333	.425	.408	.433
4				.308	.0492	.0250	.0333	.108	.375	.233	.117	.333	.500	.583	.167	.500	.583	.917	1.25	1.25
5					2.92	.00833	.0250	.0833	.333	1.92	.0833	.292	.708	2.92	.0833	.583	2.33	1.08	2.08	2.42
6						3.50	1.98	.749	.648	.433	4.34	2.30	1.30	.800	3.33	1.86	1.42	2.98	2.82	2.89
7							3.33	1.96	1.07	.740	7.43	4.32	2.80	1.37	6.50	4.37	3.20	6.92	5.67	7.62
8								4.42	2.34	1.68	4.97	8.22	6.43	4.75	11.8	10.5	8.01	14.2	13.2	14.4
9									4.75	5.57	2.68	6.56	12.8	14.8	10.3	15.9	21.0	19.7	29.8	29.8
10										40.3	1.54	3.70	16.2	49.2	7.25	20.3	51.1	25.8	56.2	54.8
11											20.2	15.0	8.50	5.39	27.6	17.2	11.5	27.2	20.8	25.4
12												21.6	19.2	14.9	41.1	35.9	28.8	53.3	46.1	54.8
13													36.8	43.0	36.5	60.2	71.5	81.2	101	115
14														134	27.5	70.8	174	93.3	200	202
15															82.9	73.9	58.2	110	98.3	116
16																120	135	182	211	257
17																	328	202	453	509
18																		337	351	469
19																			833	1,180
20																				1,960

TABLE II.- PHYSICAL PARAMETERS

(a) Wing properties

Parameter	Wing 1	Wing 2
Λ, deg	63.6	64
Span, ft	1.092	1.085
Panel span, ft	0.421	0.418
b_r, ft	0.247	0.244
x_{cg}, avg	0.442	-------
g_h, avg	0.0283	0.0216
ω_1/ω_3	0.3158	0.2991
ω_2/ω_3	0.7398	0.7196
Exposed panel mass, slugs	0.00587	0.00681
f_1, cps	108	160
f_2, cps	253	385
f_3, cps	342	535

(b) Measured mass properties of wing 1

Strip	$m\delta$, slugs	$I_\alpha\delta$, slug-ft^2	$S_\alpha\delta$, slug-ft	δ, ft	b, ft	a, ft
1	0.00184	0.000187	0.0003435	0.056	0.438	0.1866
2	.00188	.0001219	.000268	.0833	.360	.1434
3	.00120	.0000430	.000128	.0833	.276	.1067
4	.000674	.00001297	.0000483	.0833	.192	.0716
5	.000241	.00000173	.0000084	.0833	.108	.0358
6	.0000413	.00000005	.0000009	.0311	.0521	.0208

(c) Computed deflection properties of wing 1

Strip	h_1	h_2	h_3	α_1	α_2	α_3
1	0.00021	-0.0017	0.0044	0.00098	0.00015	-0.0064
2	.011	-.027	.039	.0267	-.0019	-.1250
3	.063	-.142	.156	.1070	.0194	-.4984
4	.194	-.284	.158	.2597	.0972	-.8955
5	.479	-.242	.116	.5970	.5022	-.6629
6	.862	.596	.662	.9311	.8892	.5918

TABLE III.- STRUCTURAL INFLUENCE COEFFICIENTS INFERRED AT CENTER OF GRAVITY OF SECTIONS OF WING 1, $\frac{ft}{lb} \times 10^5$

Deflection points	Load Points																			
	1	2	3	4	5	6	7	8	9	10	11	12	13	14	15	16	17	18	19	20
1	0.212	0.00833	0.0020	0.00183	0.00150	0.167	0.0833	0.0333	0.0250	0.0250	0.100	0.075	0.055	0.0417	0.142	0.0733	0.0558	0.150	0.117	0.117
2		.208	.0108	.00158	.00233	.158	.250	.133	.0833	.0542	.317	.167	.125	.0583	.175	.158	.0917	.217	.200	.333
3			.208	.00750	.00833	.0375	.125	.325	.100	.0917	.267	.458	.233	.192	.417	.333	.233	.375	.333	.342
4				.267	.180	.0367	.0642	.125	.267	.333	.127	.333	.717	.917	.417	.617	.817	.833	.967	1.06
5					1.42	.0333	.0583	.0858	.367	1.92	.0458	.187	1.04	2.08	.292	.933	1.40	.758	1.23	1.25
6						3.12	1.98	.758	.587	.433	4.04	2.25	1.21	.825	3.12	1.77	1.46	2.75	2.57	3.10
7							3.33	1.96	.958	.758	6.50	4.32	2.59	1.48	6.13	4.21	3.24	6.32	5.84	7.85
8								4.42	2.12	1.73	5.18	8.22	6.04	4.88	11.4	10.2	8.26	13.7	13.3	14.8
9									5.07	6.22	2.52	6.25	13.5	16.2	9.92	17.2	21.7	20.3	28.2	27.9
10										35.0	1.57	4.25	18.2	41.1	7.38	22.1	46.0	28.7	50.6	48.5
11											16.7	14.5	8.10	6.10	24.9	16.7	12.2	25.2	22.2	28.3
12												21.6	18.7	15.6	38.3	35.1	29.4	51.2	47.2	56.7
13													40.8	51.7	35.8	64.7	79.6	85.0	109	118
14														118	29.2	75.2	152	105	183	177
15															70.0	72.7	60.4	102	99.3	113
16																132	146	183	223	265
17																	303	226	408	434
18																		339	388	502
19																			764	958
20																				1,700

TABLE IV.- COMPILATION OF TEST AND ANALYTICAL RESULTS

Wing panel behavior code:
F - flutter
E - end of flutter (dynamic pressure increasing)
D - low damping

Subscripts:
1, 2, 3 - associated with first, second, or third occurrence of flutter during test run

Wing	Test run	Point	Wing behavior	M_e	V_e/V_R	ρ_e, slugs/cu ft	μ_e	ω_α, radians/sec	ω_e, radians/sec	ω_e/ω_R	V_e, ft/sec	V_R, ft/sec	$\frac{V_e}{b_r\omega_\alpha}$	$\frac{V_R}{b_r\omega_\alpha}$	q_e, lb/ft^2	$\frac{V_e}{b_r\omega_\alpha\sqrt{\mu_e}}$	$\frac{b_r\omega_e}{V_e}$
1	1	1	F_1	0.801	0.739	0.0044	16.55	2149	1269	0.9572	736	997	1.387	1.878	1181	0.3409	0.4259
1	2	1	F_1	.856	.754	.0025	29.13	2149	1188	.9276	929	1233	1.751	2.323	1083	.3244	.3159
1	3	1	F_1	.873	.743	.0023	31.67	2149	1125	.8836	948	1276	1.785	2.403	1027	.3172	.2931
		2	E_1	.896	.759	.0023	31.67	2149	----	------	968	1276	1.824	2.403	1070	.3240	------
		3	F_2	.929	.785	.0023	31.67	2149	1188	.9330	1001	1276	1.886	2.403	1149	.3351	.2931
		4	E_2	.962	.806	.0023	31.67	2149	----	------	1028	1276	1.938	2.403	1218	.3443	------
1	4	1	F_1	.852	.716	.0022	33.11	2149	1144	.9012	929	1297	1.750	2.444	963	.3042	.3042
		2	E_1	.892	.755	.0023	31.66	2149	----	------	963	1276	1.814	2.403	1056	.3224	------
		3	F_2	.919	.775	.0023	31.66	2149	1181	.9280	988	1276	1.862	2.403	1113	.3308	.2952
		4	E_2	.975	.815	.0023	31.66	2149	----	------	1039	1276	1.957	2.403	1234	.3478	------
		5	D_3	1.172	1.142	.0040	18.21	2149	----	------	1178	1031	2.219	1.943	2786	.5201	------
		6	F_3	1.161	1.188	.0047	15.50	2149	2620	1.9681	1155	972	2.176	1.832	3162	.5530	.5603
1	5	1	D_1	.810	.766	.0031	23.50	2149	----	------	869	1135	1.637	2.138	1164	.3377	------
		2	F_1	.795	.764	.0032	22.76	2149	1257	.9663	857	1121	1.614	2.112	1184	.3383	.3623
1	6	1	F_1	.909	.750	.0022	33.11	2149	1152	.9082	973	1297	1.832	2.444	1047	.3185	.2924
		2	E_1	.958	.783	.0022	33.11	2149	----	------	1016	1297	1.914	2.444	1145	.3326	------
		3	D_2	1.231	1.174	.0040	18.21	2149	1257	.9531	1211	1031	2.281	1.943	2943	.5345	.2564
		4	F_2	1.236	1.214	.0044	16.55	2149	2513	1.8955	1209	996	2.278	1.877	3214	.5601	.5134
1	7	1	D_1	.847	.726	.0024	30.35	2149	----	------	910	1254	1.715	2.362	1008	.3114	------
		2	F_1	.905	.780	.0025	29.13	2149	----	------	962	1234	1.812	2.324	1149	.3358	------
		3	E_1	.980	.833	.0025	29.13	2149	----	------	1028	1234	1.936	2.324	1328	.3588	------
1	8	1	F_1	.810	.745	.0029	25.12	2149	1257	.9723	868	1164	1.634	2.193	1090	.3261	.3577
1	9	1	F_1	.821	.715	.0025	29.13	2149	1169	.9129	882	1234	1.662	2.324	976	.3080	.3274
		2	E_1	.973	.842	.0027	26.98	2149	----	------	1009	1198	1.900	2.256	1371	.3658	------
		3	D_2	1.087	1.063	.0041	17.76	2149	----	------	1086	1022	2.047	1.925	2402	.4857	------
		4	F_2	1.070	1.131	.0053	13.74	2149	2450	1.8285	1054	932	1.985	1.755	2926	.5355	.5741
1	10	1	F_1	.852	.701	.0022	33.11	2149	1100	.8666	909	1297	1.713	2.444	927	.2977	.2989
		2	E_1	.992	.801	.0022	33.11	2149	----	------	1039	1297	1.958	2.444	1168	.3402	------
		3	D_2	1.249	1.291	.0053	13.74	2149	----	------	1202	932	2.265	1.755	3846	.6111	------
		4	F_2	1.238	1.313	.0060	12.14	2149	3142	2.3294	1175	894	2.213	1.685	4152	.6351	.6605
1	11	1	F_1	.813	.704	.0025	29.13	2149	1150	.8981	868	1234	1.635	2.324	930	.3030	.3272
		2	E_1	.935	.796	.0025	29.13	2149	----	------	981	1234	1.849	2.324	1192	.3425	------
		3	D_2	1.152	1.126	.0042	17.34	2149	----	------	1141	1013	2.149	1.908	2745	.5161	------
		4	F_2	1.156	1.156	.0045	16.19	2149	2476	1.8643	1142	988	2.152	1.862	2917	.5350	.5355
1	12	1	F_1	.820	.680	.0022	33.11	2149	1150	.9064	882	1297	1.662	2.444	878	.2889	.3220
		2	E_1	1.068	.872	.0023	31.67	2149	----	------	1113	1276	2.096	2.403	1410	.3726	------
		3	D_2	1.294	1.338	.0051	14.28	2149	----	------	1263	944	2.380	1.779	4039	.6297	------
		4	F_2	1.281	1.353	.0056	13.01	2149	----	------	1238	915	2.332	1.724	4296	.6468	------
1	13	1	F_1	.794	.693	.0025	29.13	2149	1150	.8983	854	1233	1.610	2.323	924	.2983	.3326
		2	E_1	.967	.844	.0027	26.98	2149	----	------	1011	1198	1.905	2.256	1405	.3667	------
		3	D_2	1.063	1.089	.0045	16.18	2149	----	------	1076	988	2.027	1.862	2616	.5040	------
		4	F_2	1.044	1.137	.0054	13.49	2149	2513	1.8734	1053	926	1.983	1.744	2995	.5399	.5895
2	1	1	D_1	.918	-----	.0043	20.12	3362	1571	------	956	----	1.165	-----	1968	.2596	.4010
		2	F_1	.917	-----	.0055	15.73	3362	1652	------	899	----	1.096	-----	2467	.2764	.4484
2	2	1	D_1	.973	-----	.0052	16.64	3362	----	------	999	----	1.218	-----	2583	.2985	------
		2	F_1	.966	-----	.0066	13.11	3362	1759	------	932	----	1.137	-----	2892	.3139	.4605
2	3	1	F_1	.965	-----	.0053	16.32	3362	1678	------	1004	----	1.224	-----	2662	.3031	.4078
2	4	1	D_1	.820	-----	.0058	14.91	3362	----	------	851	----	1.037	-----	2098	.2686	------
		2	F_1	.842	-----	.0067	12.91	3362	1816	------	859	----	1.047	-----	2475	.2915	.5158

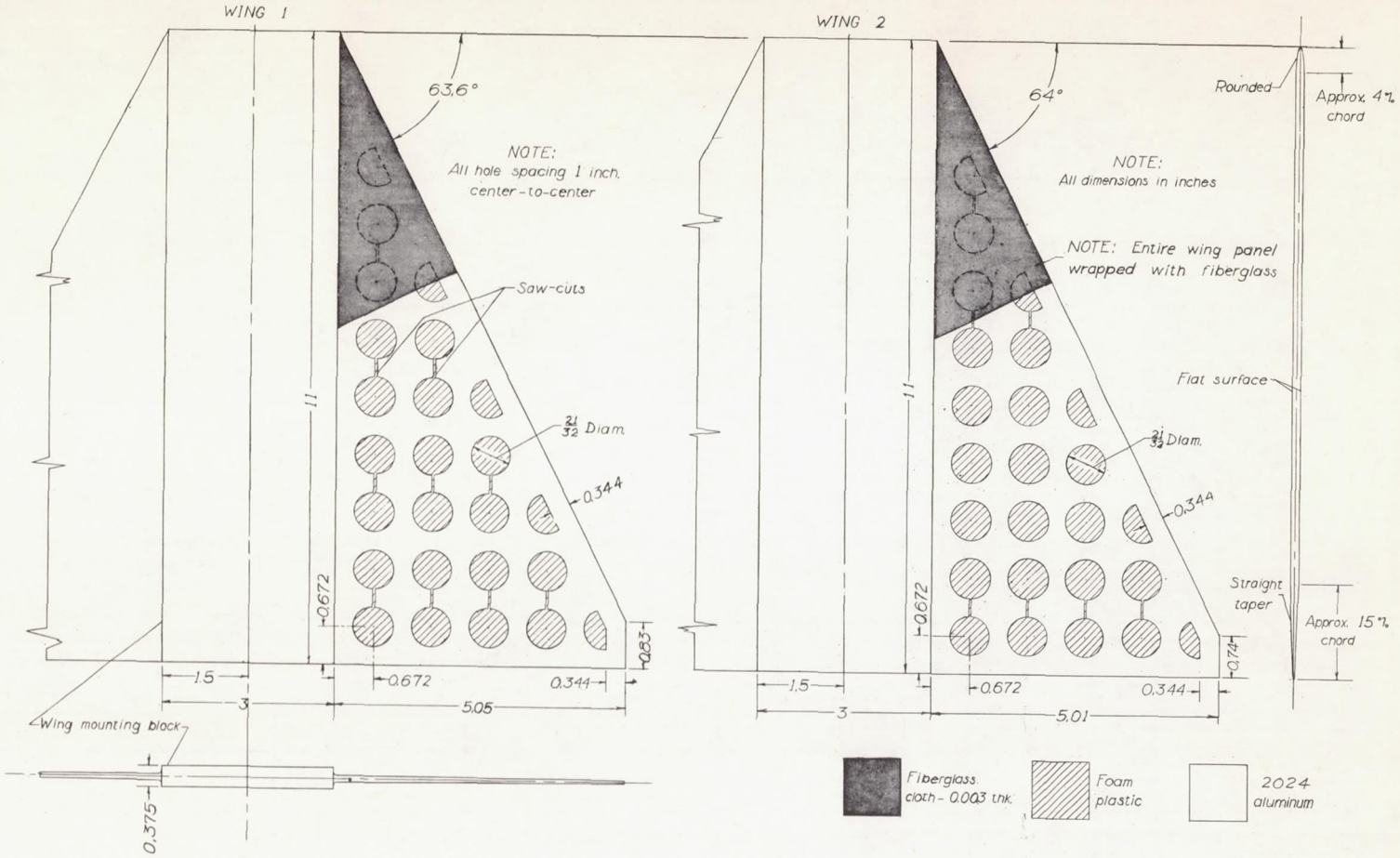

Figure 1.- Sketch of 64° delta wings showing construction details and dimensions.

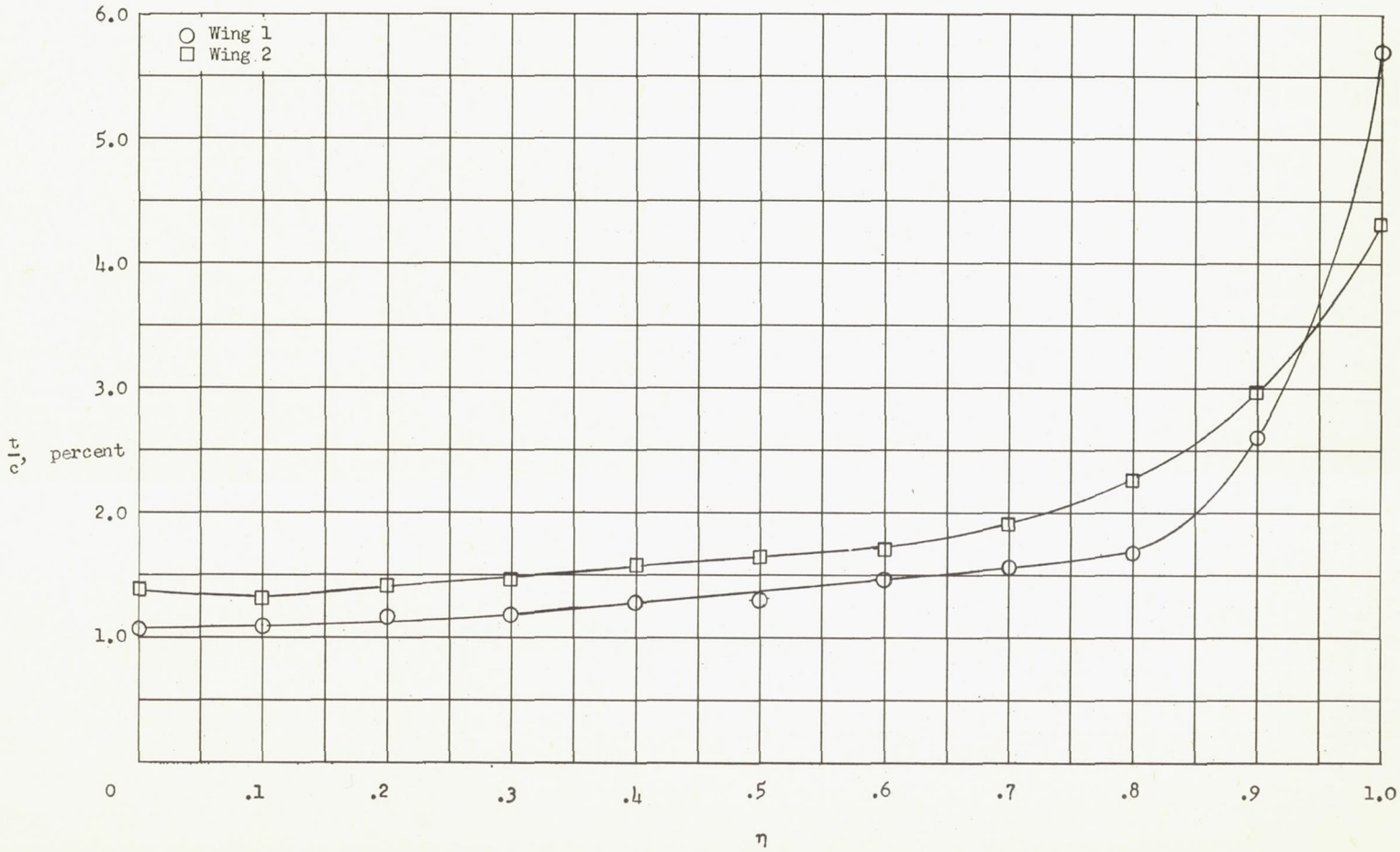

Figure 2.- Variation of ratio of average thickness (over flat part of wing) to chord along wing span for wings 1 and 2.

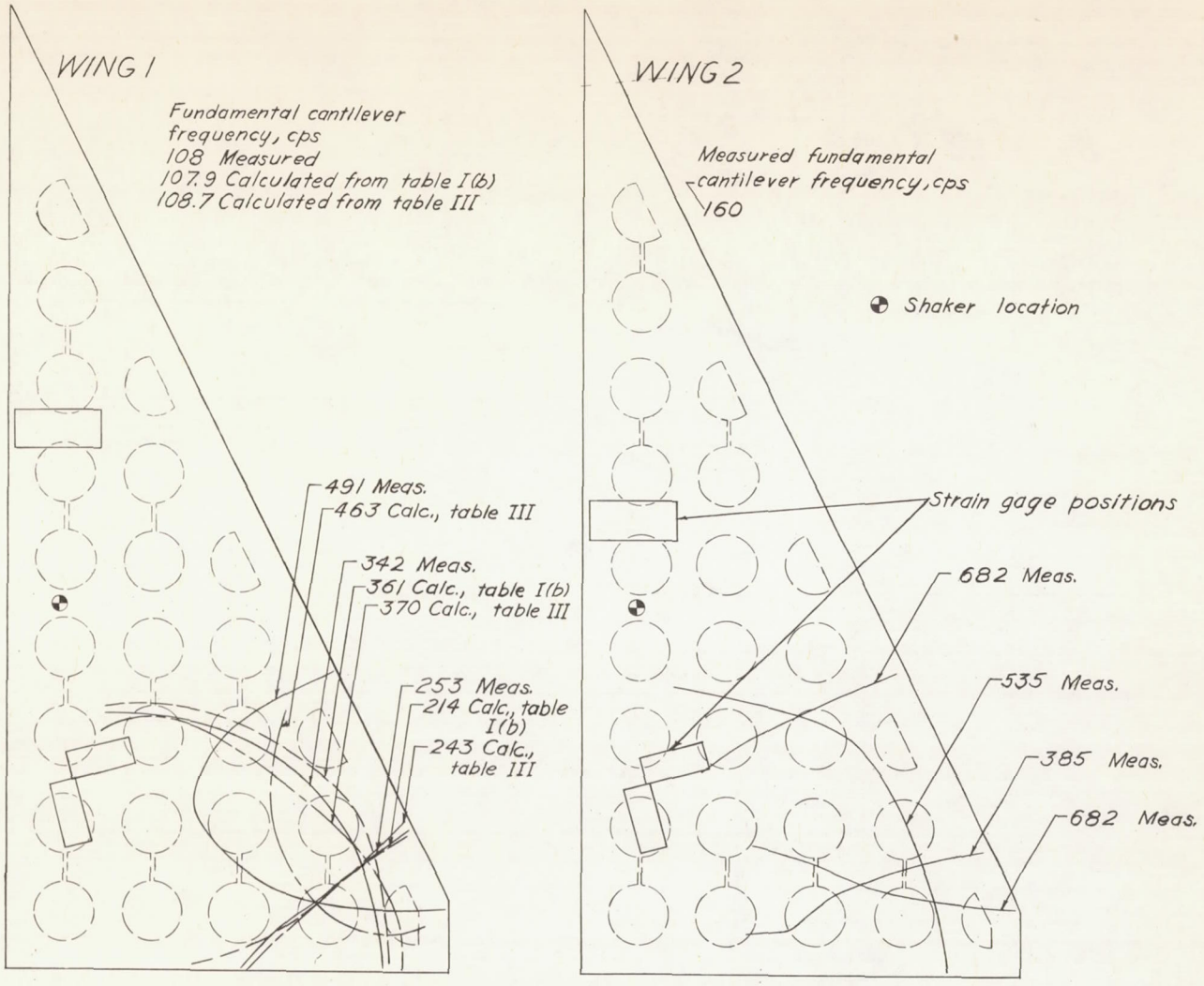

Figure 3.- Measured and calculated coupled natural vibration frequencies and node lines, shaker location, and strain-gage positions.

Strip	Streamwise distance trailing edge to strip reference axis, in.
1	7.89
2	6.48
3	4.97
4	3.46
5	1.95
6	.94

Masses of wing sections

Section	Mass (slugs X 10^3)
1	63.60
2	37.67
3	34.41
4	41.77
5	6.43
6	37.64
7	48.79
8	41.92
9	50.56
10	8.45
11	33.51
12	37.42
13	41.24
14	7.48
15	26.37
16	34.69
17	6.58
18	18.14
19	5.65
20	4.13

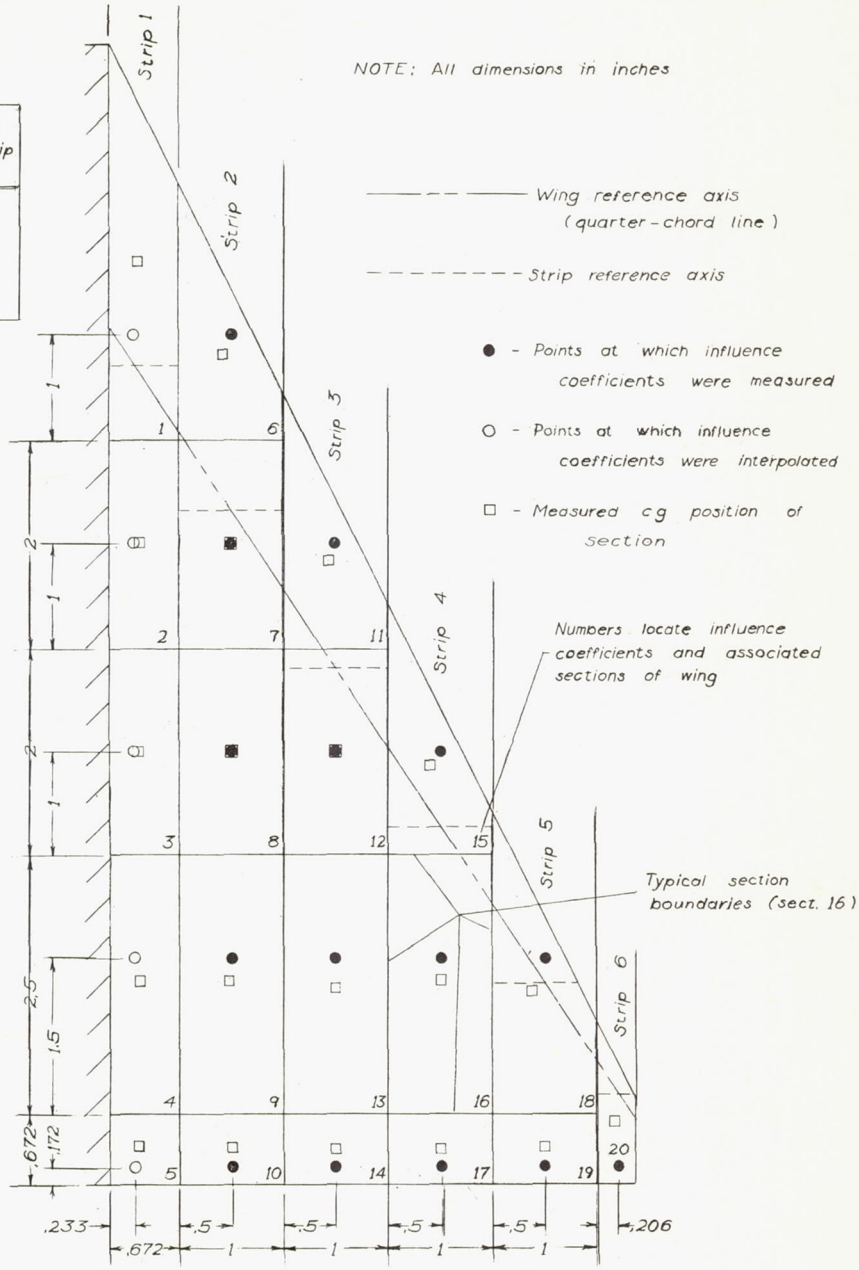

Figure 4.- Sketch of wing 1 showing strips, influence-coefficient sections, stations, and section center-of-gravity positions.

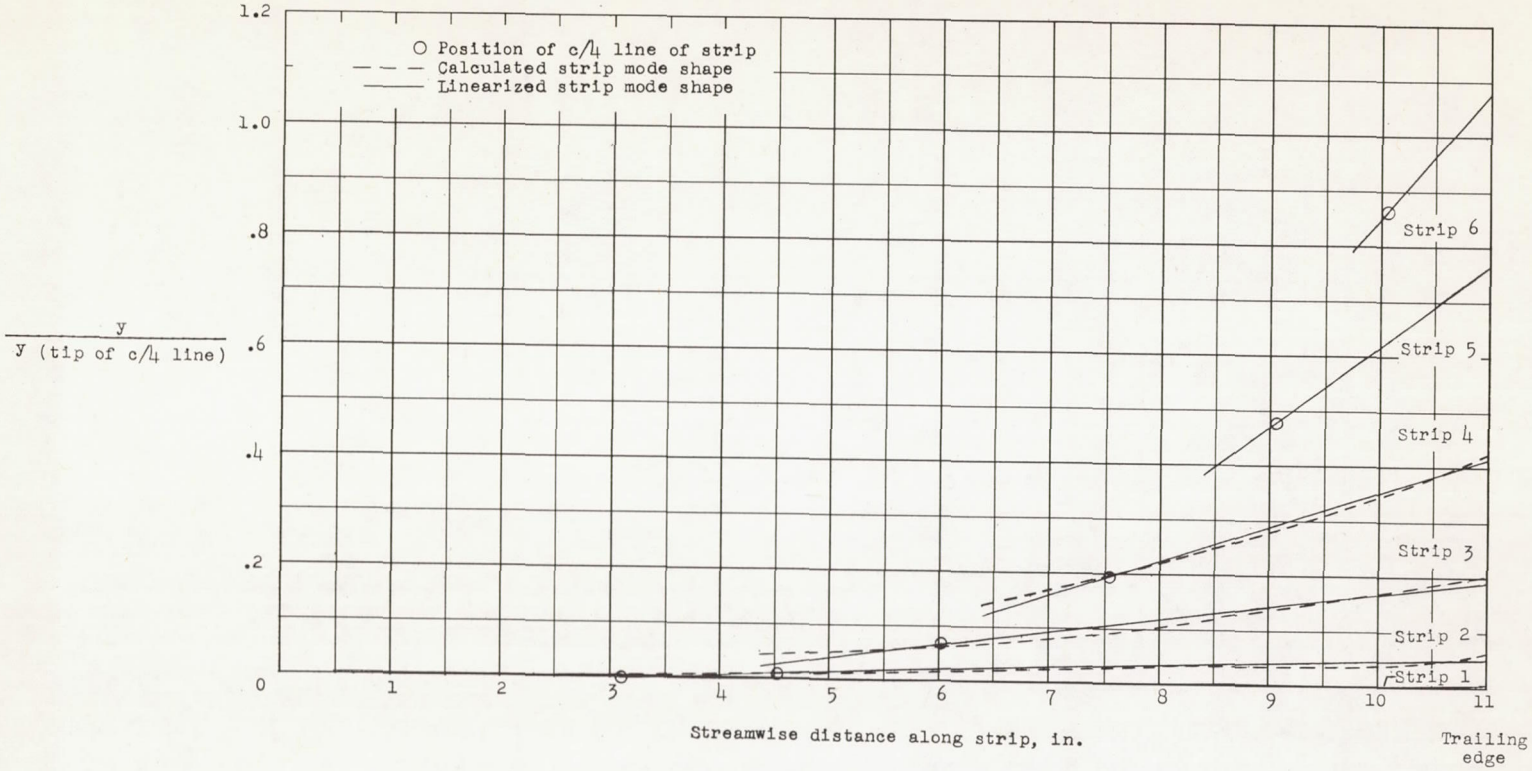

(a) First mode - calculated frequency 107.9 cps.

Figure 5.- Calculated strip mode shapes and root-mean-square strip mode shapes of wing 1.

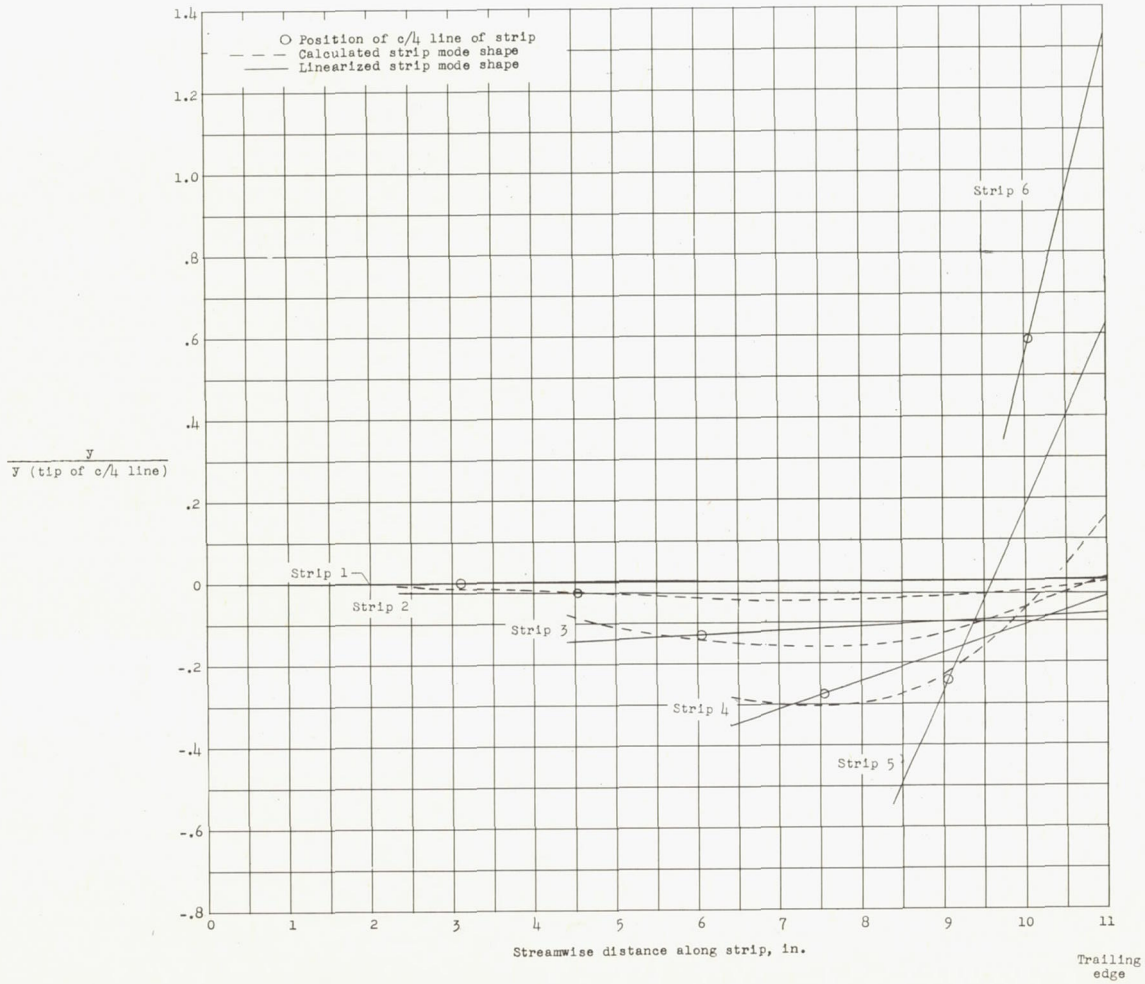

(b) Second mode - calculated frequency 214.4 cps.

Figure 5.- Continued.

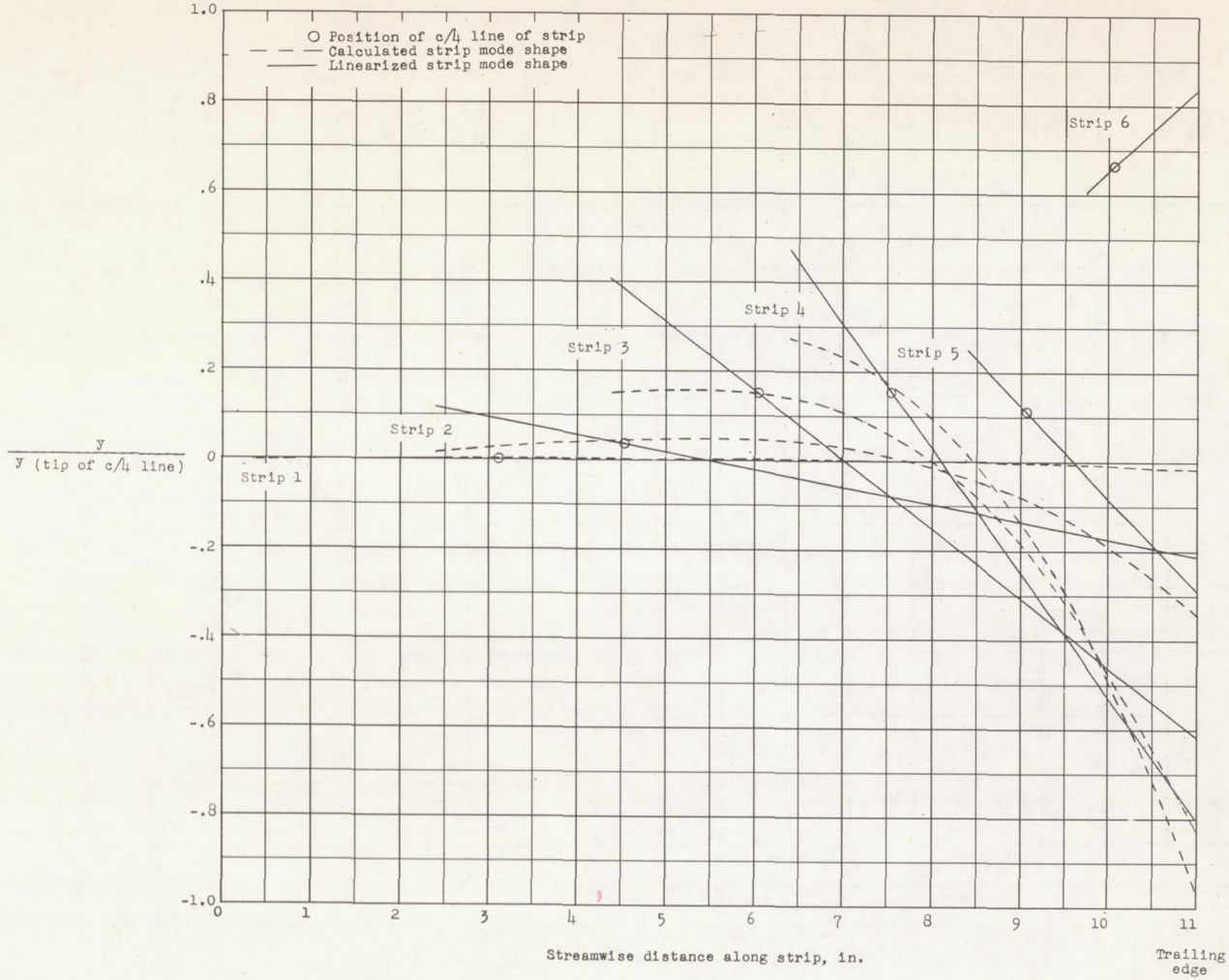

(c) Third mode - calculated frequency 360.9 cps.

Figure 5.- Concluded.

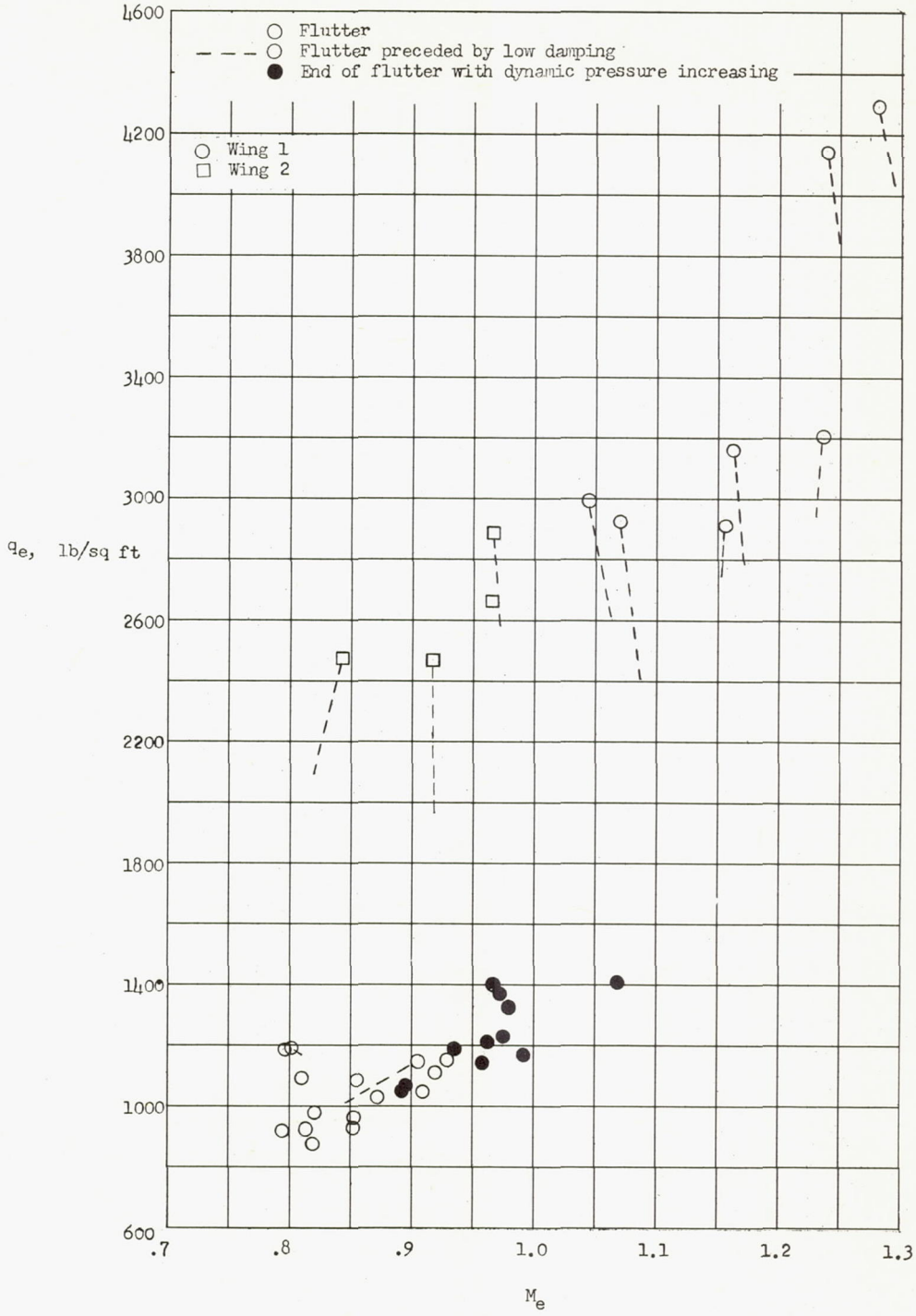

Figure 6.- Variation of dynamic pressure at flutter with Mach number for wings 1 and 2.

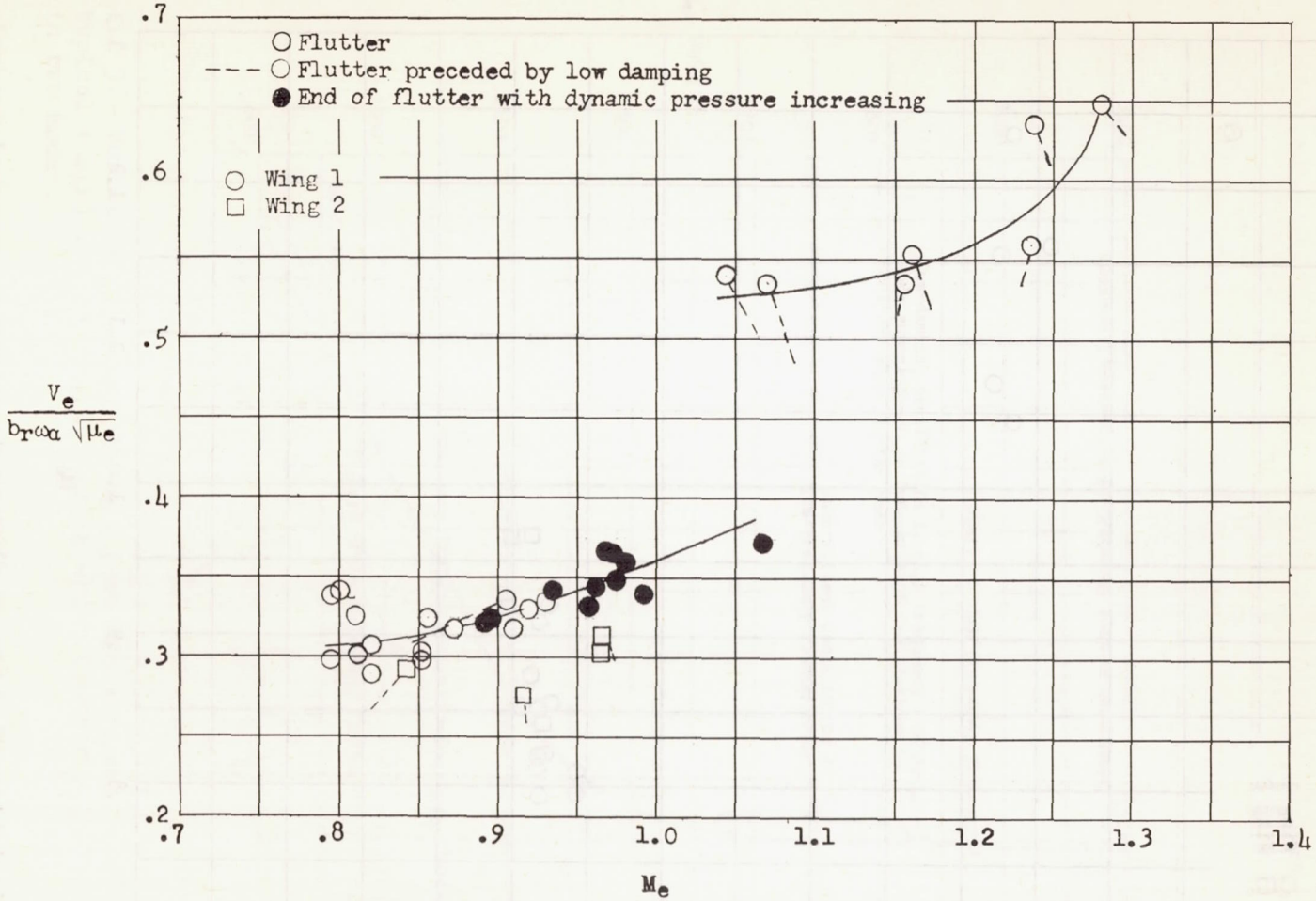

Figure 7.- Variation for wings 1 and 2 of the parameter $\frac{V_e}{b_r\omega_\alpha\sqrt{\mu_e}}$ with Mach number.

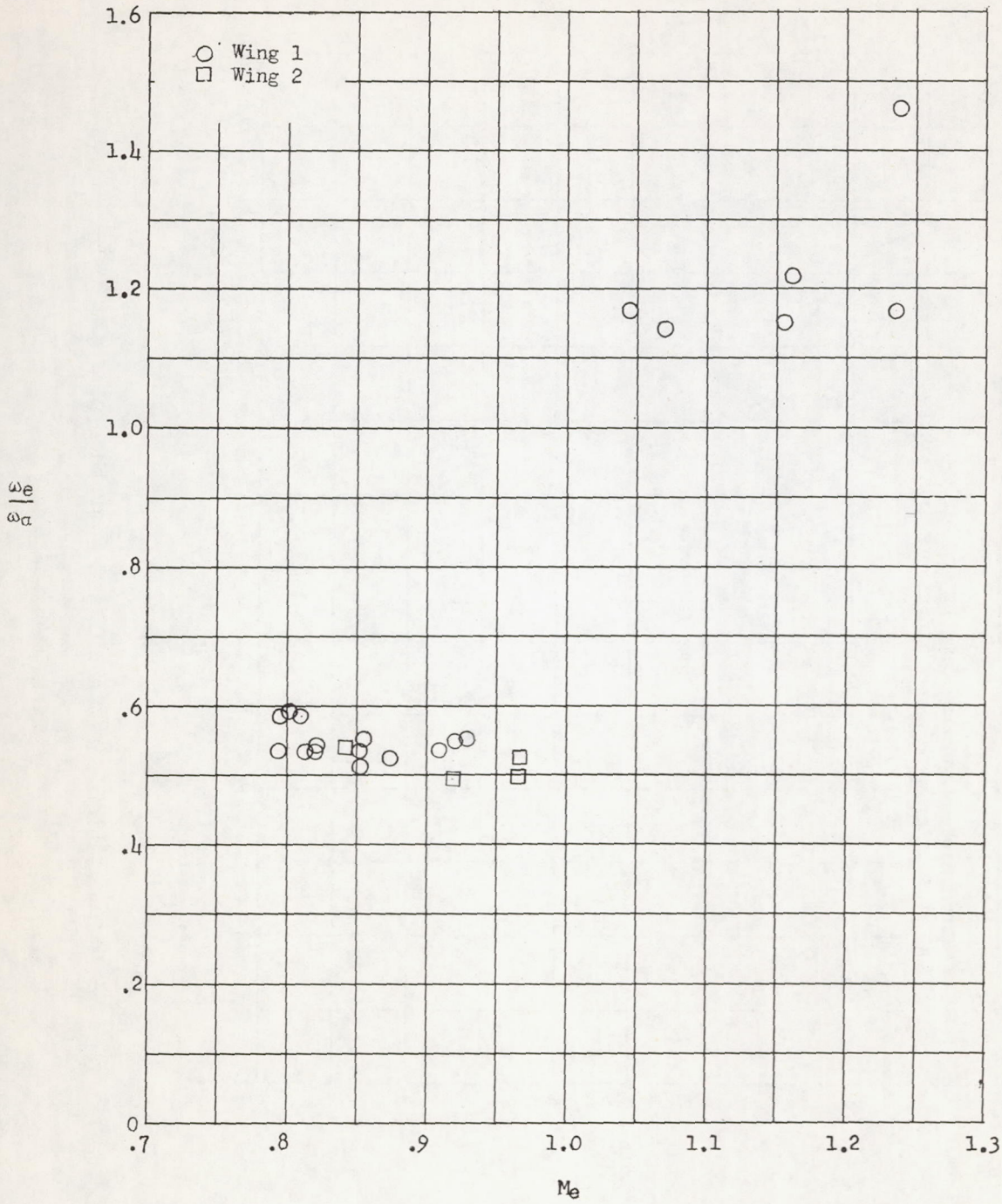

Figure 8.- Variation of ratio of flutter frequency to measured predominantly torsion frequency with Mach number for wings 1 and 2.

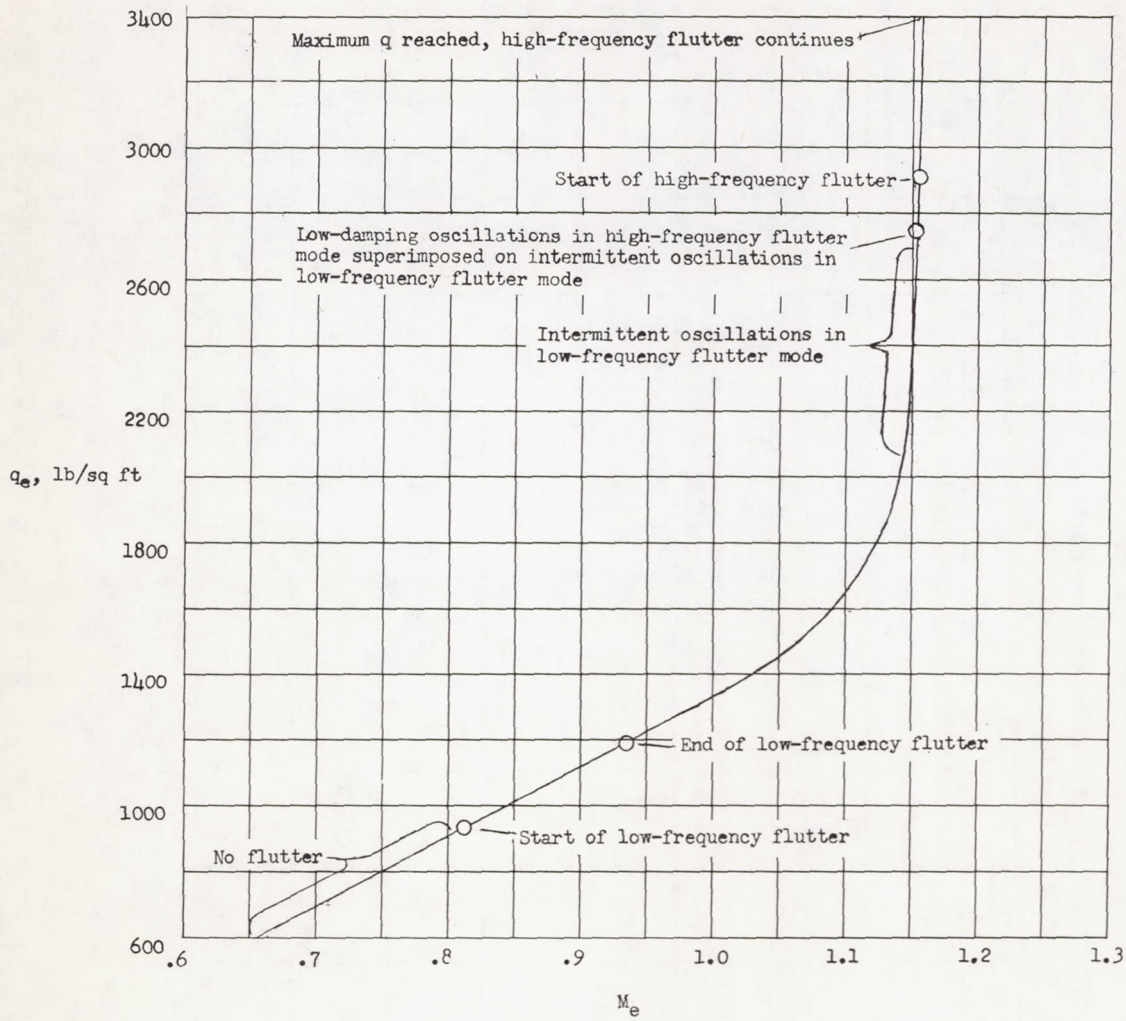

Figure 9.- Variation of tunnel dynamic pressure with Mach number for a typical tunnel run on wing 1, during which flutter apparently occurred in two modes.

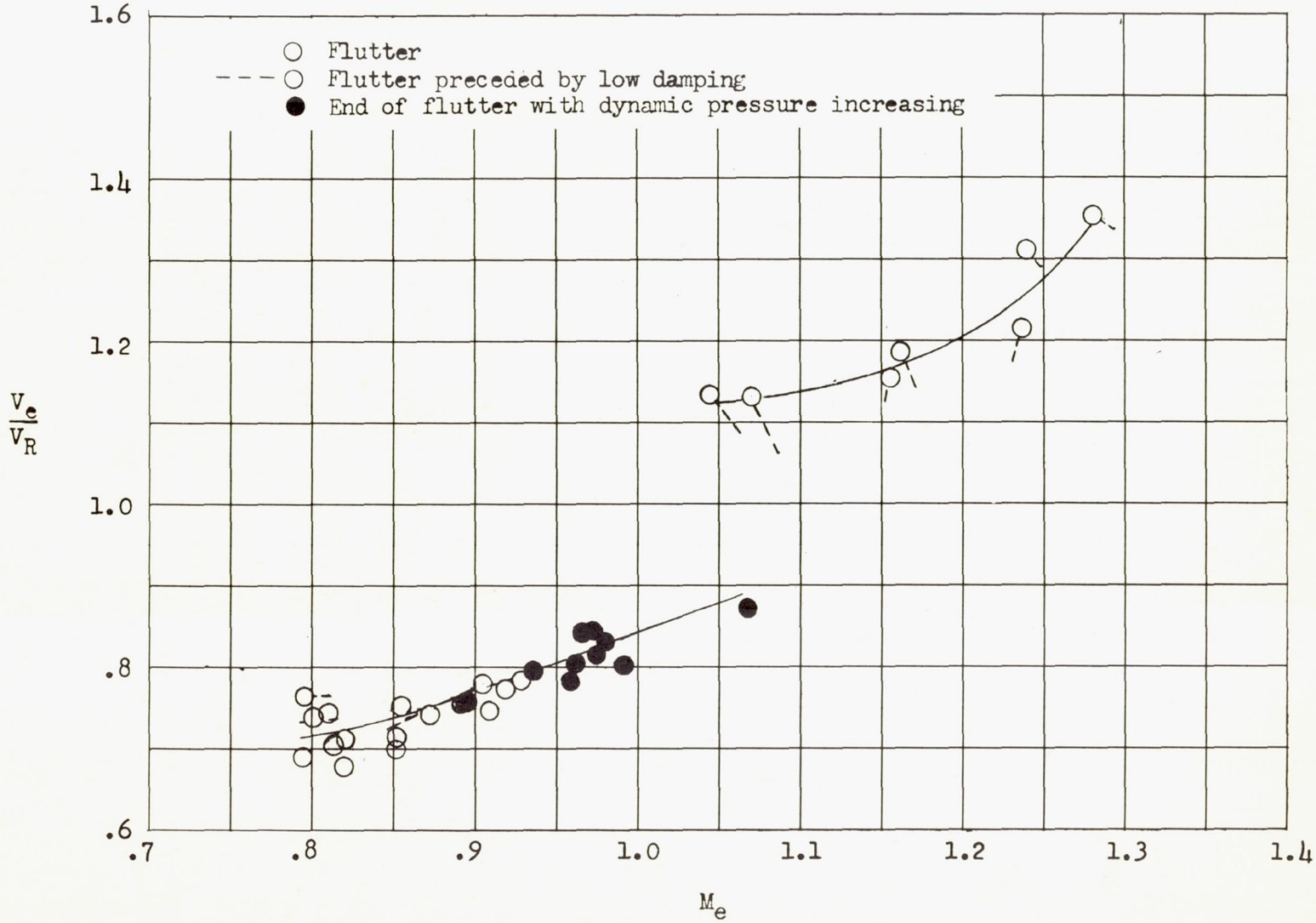

Figure 10.- Variation of flutter speed ratio with Mach number for wing 1.

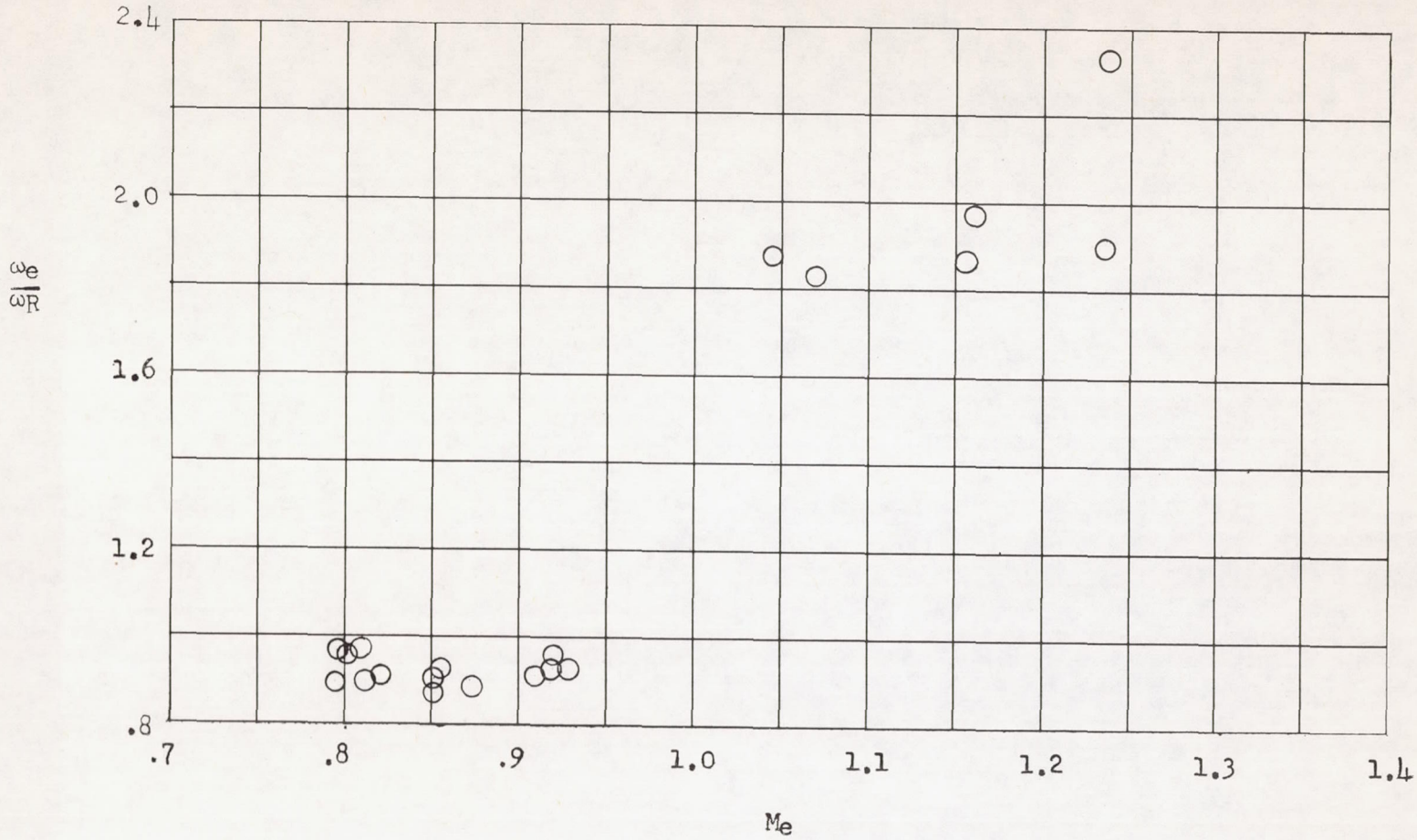

Figure 11.- Variation of ratio of experimental to calculated flutter frequency with Mach number for wing 1.

NACA - Langley Field,